Radiation Physics and Chemistry 208 (2023) 110879

Contents lists available at ScienceDirect

Radiation Physics and Chemistry

journal homepage: www.elsevier.com/locate/radphyschem

Determination of the molecular structure and spectroscopic properties of capsaicin

Mehmet Çınar [a,**], Bünyamin Alım [a,*], Zuhal Alım [b], Erdem Şakar [c]

[a] Technical Scientific Vocational School, Department of Electricity and Energy, Bayburt University, TR-69000, Bayburt, Turkey
[b] Faculty of Arts and Sciences, Department of Chemistry, University of Kırsehir Ahi Evran, Kırsehir, TR-40100, Turkey
[c] Faculty of Sciences, Department of Physics, Atatürk University, TR-25240, Erzurum, Turkey

ARTICLE INFO

Handling Editor: Dr. Chris Chantler

Keywords:
Capsaicin
Density functional theory
Spectroscopic characterization
Hirshfeld surface
Density of states

ABSTRACT

In this study, the ground state molecular structure and spectroscopic features of cis- and trans-forms of capsaicin were investigated using DFT (B3LYP) invoking 6–311++G(d,p) basis set. The optimized geometry of capsaicin was determined for the isolated molecule in a vacuum, and then the vibrational spectra –IR and Raman-were obtained, and the assignments of fundamental vibrational modes were done. By applying the GIAO method, proton and carbon chemical shifts were computed for the gas and solvated phases. Besides using the TD-DFT, the Hirshfeld surface and Molecular Electrostatic Potential surfaces were obtained and evaluated to understand the electronic properties. The Total and partial density of state (TDOS and PDOS) spectra were also examined. All obtained computational results were compared with the previously reported experimental data. A high accuracy was obtained for the ground state geometrical structure, and thus, the vibrational frequencies especially lie on the finger print region are predicted also with a high correlation. Similarly, the optimization of chemical shift values calculated by considering solvent effects with experimental data were found as high R^2 values of 0.9953 and 0.9455 for C and H atoms, respectively. This comparison shows that the DFT method precisely predicts capsaicin's molecular and spectroscopic characteristics.

1. Introduction

As a pungent ingredient in red peppers of the plant genus *Capsicum*, including chilies and jalapenos, capsaicin is a homovanillic acid derivative (8-methyl-N-vanillyl-6-nonenamide). Although it has been used in daily foods and medicinally for centuries, its definite chemical structure was determined in 1923 (Nelson and Dawson, 1923) and chemically synthesized in 1930 (Späth and Darling, 1930). Its chemical consists of a benzene ring, a polar amide group, and a long hydrophobic carbon tail. Because it is a chemical irritant, it creates a burning sensation in humans and other mammals in any tissue it comes into contact. Because of its high pungency, capsaicin affects thermoregulation, triggers autonomic reflexes, and is poorly absorbed (Patowary et al., 2017).

Moreover, several studies show that capsaicin, and related alkaloids isolated from chili peppers, called capsaicinoids, have a risk factor for duodenal (Toth et al., 1984), stomach (López-carnllo et al., 1994), gallbladder (Serra et al., 2002), and liver (Agrawal et al., 1986). On the other hand, while capsaicin is approved by the FDA and used in many fields in modern medicine, it has also been the subject of many studies to determine its different effects. Polymodal nociceptors (which respond to sensory stimuli such as noxious heat, pressure, and chemical irritation), heat nociceptors, mechano-temperature-insensitive chemociceptors, and heat receptors are known to be capsaicin-sensitive fibers (Abdel--Salam, 2014). Repeated application of capsaicin (or higher concentration) results in desensitization and low responsiveness of polymodal nociceptors to other stimuli. The peripheral use of capsaicin for chronic pain syndromes is due to this desensitizing effect. In addition, capsaicin is used in topical gels and creams to reduce rheumatoid arthritis and uremic pruritus and relieve persistent neuropathic pain. There are completed and ongoing clinical trials for using capsaicin as an agent in treating musculoskeletal pain, postoperative pain, acute/chronic neuropathic pain, and rheumatoid arthritis (Vadivelu et al., 2010). In addition, studies examining the anti-obesity (Kang et al., 2007), analgesic (Brederson et al., 2013; Simone et al., 1989), anti-inflammatory (Kim et al., 2003), and antioxidant (Galano and Martínez, 2012) effects of capsaicin are included in the literature. At different tumor stages

* Corresponding author.
** Corresponding author.
E-mail addresses: cnr.mehmet@gmail.com (M. Çınar), balim@bayburt.edu.tr (B. Alım).

https://doi.org/10.1016/j.radphyschem.2023.110879
Received 23 November 2022; Received in revised form 21 February 2023; Accepted 26 February 2023
Available online 11 March 2023

of cancer – initiation, progression, metastases – capsaicin exerts anti-cancer activity by targeting cancer-related genes and multiple signaling pathways. Activation of Apoptosis is one of the anticancer mechanisms of capsaicin. A major barrier to cancer development and progression is Apoptosis, but many types of cancer develop anti-apoptic pathways, making cancer cells resistant to Apoptosis. It has been reported that capsaicin induces Apoptosis in more than 40 different cancer cell lines (Bley et al., 2012), including lung (Athanasiou et al., 2007), liver (Y. S. Lee et al., 2009), leukemia (Ito et al., 2004), prostate (Mori et al., 2006), bladder (J. S. Lee et al., 2004), colon (Young et al., 2007), pancreatic (Pramanik et al., 2011) and skin (Hail and Lotan, 2002) cancers, without harming normal cells. Athanasiou et al. have proven that capsaicin exhibits anti-angiogenic properties both *in vitro* and *in vivo* (Athanasiou et al., 2007). It has been reported that capsaicin exhibits anti-invasive and anti-migration activities by modulating the signaling pathways related to cell invasion and migration (Price and Collard, 2001; Shin et al., 2008; Venier et al., 2015).

Spectroscopic characterization is also included in the massive literature on capsaicin studies. The FT-IR spectrum of capsaicin from callus derived from different explants of local hot pepper (Capsicum annuum L.) was recorded (El Kaaby Ekhlas A. et al., 2016). Leela et al. recorded the FT-IR spectrum of capsaicin in the solid phase and compared it with the DFT calculations (Sherin Percy Prema Leela et al., 2015). The Raman spectrum of solid phase and Surface Enhanced Raman Spectroscopy (SERS) spectrum of capsaicin adsorbed on silver nanorod substrate Tian et al. (2018) supported by DFT calculations. ^{1}H and ^{13}C NMR spectra were recorded and published by Lin et al. for cis- and trans-capsaicin in chloroform solvent (Lin et al., 1993). Bora et al. developed a sensitive ^{1}H quantitative NMR technique for capsaicin and total capsaicinoid in dried chile pepper and chile pepper oleoresin and applied it to 15 samples (Bora et al., 2021). Siudem et al., characterized the solid-state structure of capsaicin using ^{13}C and ^{15}N MAS NMR spectroscopy (Siudem et al., 2017). Qais et al., recorded the UV–Vis spectrum of capsaicin in their study, examining capsaicin's interaction with calf thymus DNA (Qais et al., 2017).

Although computational studies have been carried out for capsaicin before, there is no study in which geometric optimization and spectroscopic characterization are discussed in detail. In this study, cis- and trans-forms of capsaicin were analyzed by DFT (B3LYP) and using the 6–311++G(d,p) basis set and compared with reported experimental data. The optimum geometry was determined, and IR and Raman spectra were obtained by evaluating their vibrational modes, NMR and electronic properties were examined by investigating different solvent environments as well as the gas phase.

2. Quantum chemical calculations

Density functional theoretical (DFT) calculations were performed on isolated *cis*- and *trans*-capsaicin using the B3LYP functional in combination with the 6–311++G(d,p) basis set to achieve complete geometry optimization for the ground state, normal mode analysis, and NMR chemical shifts (Becke, 1998; C. Lee et al., 1988; Perdew and Wang, 1992). In this function, the geometric structure of the isolated molecule at the lowest energy level is determined by Berny's optimization algorithm using redundant internal coordinates. In the calculation of harmonic vibration wave numbers, analytical second derivatives are used to verify the convergence to the minimum on the potential energy surface. The calculated harmonic vibrational wavenumbers are higher when systematic errors due to basis set incompleteness, neglect of electron correlation, or vibrational anharmonicity are considered (Scott and Radom, 1996). Therefore, the calculated harmonic vibration wave number was reduced by two scaling factors, 0.983 for those up to 1700 cm^{-1} and 0.958 for those larger than 1700 cm^{-1} (Cinar et al., 2011; Karabacak et al., 2010; Kurt et al., 2011). Based on the obtained geometric structure, ^{1}H and ^{13}C NMR chemical shifts were estimated using the GIAO (Gauge Invariant Atomic Orbital) method in the gas phase and solvated phase (DMSO and Chloroform) (Dltchfield, 2003; Wolinski et al., 2002). The excited-state electronic properties such as HOMO-LUMO energies, dipole moment, absorption wavelengths, and oscillator strengths were determined by the time-dependent DFT (TD-DFT) method. This method combines the advantages of DFT and time-dependent formalism, allowing the excited state properties to be determined accurately (Adamo et al., 1999; Bauernschmitt and Ahlrichs, 1996; Casida et al., 1998; Chong, 1995; Jamorski et al., 1998; Karabacak et al., 2009; Petersilka et al., 1996; Van Gisbergen et al., 1998). However, spatially expanded and charge-transfer excited states are known failures of the TD-DFT method (Dreuw and Head-Gordon, 2004). The Gaussian 09 program package (Frisch et al., 2009) was used for the calculations. The Hirshfeld surface analysis was determined using the existing *.cif file of capsaicin crystal (David et al., 1998) with the Crystalexplorer 3.1 program package (Turner et al., 2017). The density of states (DOS) was calculated using GaussSum 3.0.2. software (O'Boyle et al., 2008).

3. Results and discussion

3.1. Molecular geometry

The geometric structure obtained for *cis*-capsaicin and its chemical structure is given in Fig. 1, while the structure obtained for the *trans*-form of capsaicin is given as supplementary materials in Fig. S1. The energy of the obtained structure was calculated as approximately −982 Hartree (−26720 eV). The cis-capsaicin molecule's optimized structural parameters (bond lengths, bond angles, and dihedral angles) are listed in Table 1, and the atomic numbering is in accordance with Fig. 1. The same parameters obtained for the *trans*-capsaicin are given as supplementary data in Table S1.

If there is experimental data on the geometric structure of a compound, these data are used as input parameters for the theoretical minimum energy geometric optimization of the molecule. Thus, it is

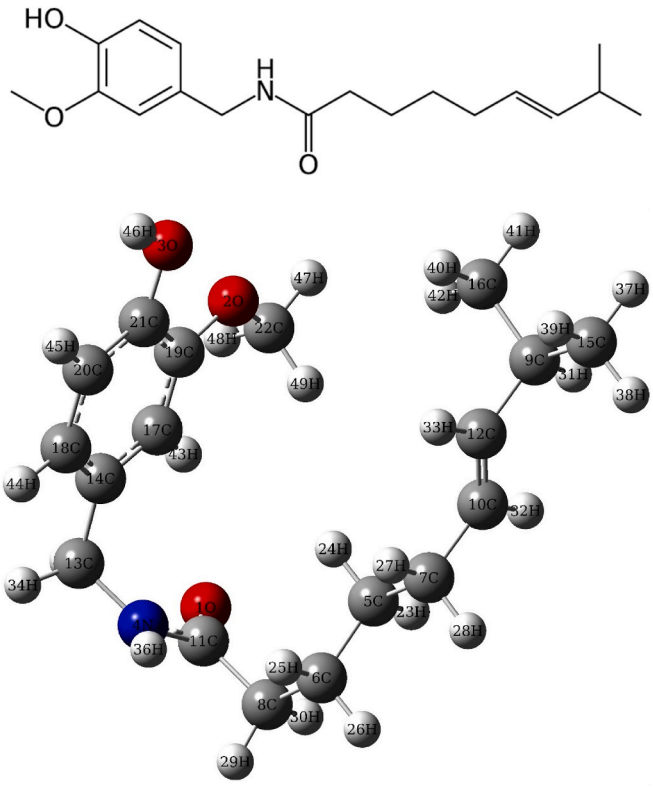

Fig. 1. Optimized geometric structure of *cis*-Capsaicin by DFT (B3LYP)/6311++G(d,p) (E = - 982 Hartree = - 26720 eV).

Table 1
Computed geometrical parameters of *cis*-Capsaicin in comparison with experimental data, bond lengths in Angstrom (Å), angles in degrees (°).

Bond Lengths	Exp. [a]	B3LYP	Bond Lengths	Exp. [a]	B3LYP	Bond Angles	Exp. [a]	B3LYP	Bond Angles	Exp. [a]	B3LYP	Dihedral Angles	Exp. [a]	B3LYP
O(1) = C (11)	1.240	1.224	C(12)–H (33)	1.000	1.092	C(13)-C (14)-C(18)	120.0	119.0	C(11)-C(8)-H(29)	109.5	108.7	C(22)-O(2)-C (19)-C(17)	6.6	1.2
O(2)–C (19)	1.370	1.359	C(13)–H (34)	1.000	1.093	C(14)-C (17)-C(19)	120.0	121.2	C(11)-C(8)-H(30)	109.5	106.2	C(22)-O(2)-C (19)-C(21)	−173.4	−178.4
O(2)–C (22)	1.420	1.423	C(13)–H (35)	1.000	1.091	C(14)-C (18)-C(20)	120.0	120.2	H(29)-C(8)-H(30)	109.5	107.5	C(13)-N(4)-C (11)-C(8)	−168.0	177.1
O(3)–C (21)	1.370	1.367	C(15)–H (37)	1.000	1.094	O(2)-C (19)-C(17)	120.0	124.9	C(12)-C(9)-H(31)	109.5	107.9	C(11)-N(4)-C (13)-C(14)	−100.8	−90.8
N(4)–C (11)	1.350	1.367	C(15)–H (38)	1.000	1.093	O(2)-C (19)-C(21)	120.0	115.9	C(15)-C(9)-H(31)	109.4	108.1	C(13)-N(4)-C (11) = O(1)	12.0	−3.9
N(4)–C (13)	1.460	1.466	C(15)–H (39)	1.000	1.095	C(17)-C (19)-C(21)	120.0	119.2	C(16)-C(9)-H(31)	109.4	108.3	C(18)-C(14)-C (13)-N(4)	−160.5	−104.7
C(5)–C(6)	1.540	1.533	C(16)–H (40)	1.000	1.095	C(18)-C (20)-C(21)	120.0	120.8	C(7)-C(10)-H(32)	120.0	115.9	C(18)-C(14)-C (17)-C(19)	0.0	0.4
C(5)–C(7)	1.540	1.539	C(16)–H (41)	1.000	1.094	O(3)-C (21)-C(19)	120.0	117.3	C(12)-C (10)-H(32)	120.0	118.7	C(13)-C(14)-C (18)-C(20)	−180.0	179.1
C(6)–C(8)	1.540	1.541	C(16)–H (42)	1.000	1.093	O(3)-C (21)-C(20)	120.0	123.2	C(9)-C(12)-H(33)	120.0	115.5	C(17)-C(14)-C (13)-N(4)	19.6	−74.8
C(7)–C (10)	1.480	1.504	C(17)–H (43)	1.000	1.082	C(19)-C (21)-C(20)	120.0	119.5	C(10) = C (12)–H(33)	120.0	118.8	C(17)-C(14)-C (18)-C(20)	0.0	−0.4
C(8)–C (11)	1.510	1.527	C(18)–H (44)	1.000	1.085	N(4)-C (13)-H (34)	109.4	107.8	C(14)-C (13)-H(34)	109.5	109.9	C(13)-C(14)-C (17)-C(19)	180.0	−179.1
C(9)–C (12)	1.480	1.507	C(20)–H (45)	1.000	1.087	N(4)-C (13)-H (35)	109.5	106.4	C(14)-C (13)-H(35)	109.5	110.5	C(14)-C(17)-C (19)-C(21)	0.0	−0.1
C(9)–C (15)	1.540	1.540	C(22)–H (47)	1.000	1.089	C(11)-N (4)-H(36)	118.0	118.3	H(34)-C (13)-H(35)	109.4	107.9	C(14)-C(17)-C (19)-O(2)	−180.0	−179.7
C(9)–C (16)	1.540	1.539	C(22)–H (48)	1.000	1.095	C(13)-N (4)-H(36)	120.0	117.8	C(9)-C(15)-H(37)	109.5	110.9	O(2)-C(19)-C (21)-C(20)	180.0	179.4
C(10) = C (12)	1.300	1.333	C(22)–H (49)	1.000	1.095	O(2)-C (22)-H (47)	109.5	105.6	C(9)-C(15)-H(38)	109.5	111.2	C(17)-C(19)-C (21)-O(3)	180.0	−179.9
C(13)–C (14)	1.540	1.515	Bond Angles	Exp. [a]	B3LYP	O(2)-C (22)-H (48)	109.5	111.3	C(9)-C(15)-H(39)	109.5	110.8	C(17)-C(19)-C (21)-C(20)	0.0	−0.2
C(14)–C (17)	1.400	1.405	C(19)-O(2)-C(22)	120.0	118.1	O(2)-C (22)-H (49)	109.5	111.4	C(9)-C(16)-H(40)	109.5	110.9	O(2)-C(19)-C (21)-O(3)	0.0	−0.3
C(14)–C (18)	1.400	1.390	C(21)-O(3)-H(46)	120.0	109.1	C(6)-C(5)-H(23)	109.5	109.2	C(9)-C(16)-H(41)	109.5	110.9	O(3)-C(21)-C (20)-C(18)	−180.0	−179.9
C(17)–C (19)	1.400	1.391	C(11)-N(4)-C(13)	122.0	123.0	C(6)-C(5)-H(24)	109.5	110.0	C(9)-C(16)-H(42)	109.5	111.4	C(19)-C(21)-C (20)-C(18)	0.0	−0.2
C(18)–C (20)	1.400	1.399	C(6)-C(5)-C (7)	109.5	112.7	C(7)-C(5)-H(23)	109.4	109.5	C(14)-C (17)-H(43)	120.0	118.4	C(21)-C(20)-C (18)-C(14)	0.0	0.1
C(19)–C (21)	1.400	1.413	C(5)-C(6)-C (8)	109.5	114.1	C(7)-C(5)-H(24)	109.4	109.0	C(19)-C (17)-H(43)	120.0	120.4	O(1) = C(11)-C(8)-C(6)	43.3	114.7
C(20)–C (21)	1.400	1.387	C(5)-C(7)-C (10)	109.5	113.3	H(23)-C (5)-H(24)	109.5	106.2	C(14)-C (18)-H(44)	120.0	120.4	N(4)-C(11)-C (8)-C(6)	−136.7	66.3
O(3)–H (46)	1.000	0.963	C(6)-C(8)-C (11)	109.5	114.7	C(5)-C(6)-H(25)	109.5	109.3	C(20)-C (18)-H(44)	120.0	119.4	C(11)-C(8)-C (6)-C(5)	77.5	61.2
N(4)–H (36)	0.900	1.008	C(12)-C(9)-C(15)	109.5	110.8	C(5)-C(6)-H(26)	109.5	109.3	C(18)-C (20)-H(45)	120.0	120.0	C(8)-C(6)-C (5)-C(7)	158.5	178.3
C(5)–H (23)	1.000	1.097	C(12)-C(9)-C(16)	109.5	110.9	C(8)-C(6)-H(25)	109.5	110.2	C(21)-C (20)-H(45)	120.0	119.2	C(6)-C(5)-C (7)-C(10)	164.2	177.7
C(5)–H (24)	1.000	1.095	C(15)-C(9)-C(16)	109.5	110.7	C(8)-C(6)-H(26)	109.5	108.0	H(37)-C (15)-H(38)	109.4	108.2	C(5)-C(7)-C (10)-C(12)	−144.7	119.2
C(6)–H (25)	1.000	1.097	C(7)–C(10) = C(12)	120.0	125.4	H(25)-C (6)-H(26)	109.4	105.7	H(37)-C (15)-H(39)	109.4	107.7	C(7)-C(10)-C (12)-C(9)	180.0	180.0
C(6)–H (26)	1.000	1.096	O(1) = C (11)–N(4)	123.0	122.4	C(5)-C(7)-H(27)	109.5	109.6	H(38)-C (15)-H(39)	109.5	107.8	C(10)-C(12)-C (9)-C(15)	21.7	116.5
C(7)–H (27)	1.000	1.096	O(1) = C (11)–C(8)	116.0	122.4	C(5)-C(7)-H(28)	109.5	108.5	H(40)-C (16)-H(41)	109.5	107.7	C(10)-C(12)-C (9)-C(16)	−98.4	−20.2
C(7)–H (28)	1.000	1.099	N(4)-C(11)-C(8)	121.0	115.2	C(10)-C (7)-H(27)	109.4	109.5	H(40)-C (16)-H(42)	109.4	107.5			
C(8)–H (29)	1.000	1.096	C(9)–C(12) = C(10)	120.0	125.8	C(10)-C (7)-H(28)	109.5	109.3	H(41)-C (16)-H(42)	109.5	108.3			
C(8)–H (30)	1.000	1.091	N (4)-C (13)-C(14)	109.5	114.1	H(27)-C (7)-H(28)	109.5	106.5	H(47)-C (22)-H(48)	109.5	109.5			
C(9)–H (31)	1.000	1.097	C(13)-C (14)-C(17)	120.0	119.6	C(6)-C(8)-H(29)	109.4	109.4	H(47)-C (22)-H(49)	109.4	109.5			
C(10)–H (32)	1.000	1.091	C(18)-C (14)-C(17)	120.0	121.3	C(6)-C(8)-H(30)	109.5	110.1	H(48)-C (22)-H(49)	109.5	109.3			
r.m.s.		0.015									3.4			

[a] David et al. (1998).

aimed that the optimum structure to be obtained will be closest to the experimentally determined one because all other calculations are made according to the optimum structure obtained and therefore affect all calculations. In the literature, it is seen that the crystal structure of capsaicin was determined experimentally and reported by David et al. (1998). Therefore, the input parameters of the studied molecule were first entered according to the experimental data, and the molecule was optimized. However, when the vibrational frequencies were calculated according to the obtained structure, one negative frequency was calculated, indicating that the optimum structure was not in the ground energy state. For this reason, the calculations were repeated by arranging the input parameters more appropriately, and this geometric structure was also used for all other computations since all vibration frequencies were positive. In this study, the parameters obtained by quantum chemical calculation are given by comparing them with the experimental data mentioned above. As seen in the bottom row of Table 1, the root mean square (r.m.s.) values were given without considering the hydrogen bonds (because in the determination of crystal structures by X-ray analysis, bonds such as C–H and N–H are usually set to a fixed value), and the r.m.s. value was found as 0.015 Å for bond lengths and 3.4° for bond angles. These values show that there is a slight deviation and a strong correlation between the experimental and computational data. On the other hand, to understand how the theoretically obtained structure and the experimental one fit well, it is necessary to look at the dihedral angles of the structures first. However, comparing here, it should be noted that the theoretical calculations were performed for the isolated molecule and in the gas phase, and the experimental results were obtained for the crystal structure. Therefore, it is expected that the calculations that do not include intermolecular interactions will differ from the experimental ones, especially for electron acceptor or electron donor atoms and, accordingly, the bond length, bond angles, and dihedral angles in which these atoms are located. When evaluated in this manner, the expected differences can be seen in this study as the strong intermolecular bonds originate from N and O atoms, and these intermolecular bonds affect the geometric structure. The differences in the values of the dihedral angles of these atoms in Table 1 are due to this effect. This different positioning in the molecular structure also affects other atoms, and due to interactions between atoms, differences are observed in the remaining parts of the molecule between the theoretical and experimental ones. Therefore, it is usual for some shifts in the theoretical calculations relative to the experimental data since all other calculations are performed according to this structure. However, when a comparison is made for bond lengths and bond angles, the differences can be seen to be very low and satisfactory, demonstrating the success of DFT in quantum chemical calculations. For example, the difference is 0.016 Å for the C═O double bond length, while it is only 0.003 Å for the C–O bond. In addition, acceptable differences such as 0.017 Å and 0.006 Å were found for C–N bonds. A quick look at the C–C bonds, it can be seen that some bond lengths matched with the experimental data perfectly (for instance, C_9–C_{15}, C_5–C_7, C_6–C_8, C_9–C_{18}, C_{18}–C_{20}), while others were calculated at relatively larger values (C_7–C_{10} and $C_{10} = C_{12}$). The C_{13}–C_{14} bond was calculated as 0.025 Å shorter than the experimental one and found to be 1.515 Å. In general, a good correlation for bond lengths is obtained with the R^2-value found to be 0.99325 (including hydrogen bonds) and is given in Fig. 2. When the bond angles between atoms are compared, the most notable differences are the angles in which the O and N atoms are located. O_1═C_{11}–C_8 bond angle was calculated as 6.4° larger, and the most significant difference was observed for this angle. The discrepancy of the N_4–C_{11}–C_8 and C_9–$C_{12} = C_{10}$ angles was found to be 5.8°, and this difference was due to the calculation of a smaller value for the first one and the latter; it is due to the calculation of a larger value. It should also be noted that since all other calculations are performed according to this structure, it is usual

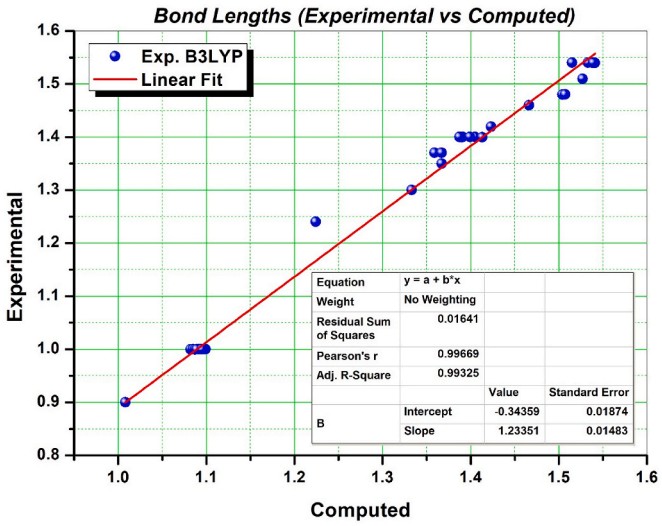

Fig. 2. Correlation between the experimentally obtained vs computed bond lengths for *cis*-Capsaicin.

for some shifts in the theoretical calculations relative to the experimental data.

3.2. Vibrational analysis

The purpose of vibration analysis is to find vibrational modes associated with the molecular structure of the studied compound. Therefore, Infrared and Raman spectra of capsaicin were obtained by quantum chemical computation methods and vibration modes were determined by visualizing with GaussView. Capsaicin consists of 49 atoms; accordingly, 141 (3N-6, N indicates the number of atoms) vibrational frequencies have been obtained. The vibrational frequencies values, IR intensity (I_{IR}), Raman Activity (A_{Ra}), Raman Intensity (I_{Ra}), and experimentally obtained FT-IR (El Kaaby Ekhlas A. et al., 2016; Sherin Percy Prema Leela et al., 2015), and Raman (Tian et al., 2018) -given in *italics*-values are presented in Table 2 (for *cis*-capsaicin) and Supplementary Table S2 (for *trans*-capsaicin). Here, the Raman activities were obtained directly with the used software, and the Raman intensities were calculated using the obtained Raman activities, with the following formula derived from the density theory of Raman scattering (Keresztury, 2006; Keresztury et al., 1993), and normalized to 1.

$$I_i = \frac{f(\upsilon_0 - \upsilon_i)^4 S_i}{\upsilon_i[1 - exp(-hc\upsilon_i/kT)]}$$

where υ_0 is the exciting laser wavenumber in cm^{-1} (in this work, we have used the excitation wavenumber $\upsilon_0 = 9398.5\ cm^{-1}$, which corresponds to the wavelength of 1064 nm of an Nd: YAG laser), υ_i the vibrational wavenumber of the *i*th normal mode (cm^{-1}), while S_i is the Raman scattering activity of the normal mode υ_i, f (is a constant equal to 10^{-12}) is a suitably chosen common normalization factor for all peak intensities. *h, k, c,* and *T* are Planck and Boltzmann constants, speed of light, and temperature in Kelvin, respectively.

The experimental FT-IR spectrum of capsaicin was recorded in the range of 4000-400 cm^{-1} by El Kaaby Ekhlas et al. (El Kaaby Ekhlas A. et al., 2016) and Leela et al. (Sherin Percy Prema Leela et al., 2015). The Raman spectrum was recorded by Tian et al. (2018) in the range of 1800-0 cm^{-1} in the solid phase, and these data were used as a reference in this study. In the present study, the predicted IR and Raman spectra of *cis*-capsaicin are shown in Fig. 3. Accordingly, the critical vibrational

Table 2
Calculated vibrational wavenumbers in comparison with experimental data, IR and Raman Intensities, Raman activities of *cis*-Capsaicin.

No	Frequencies							Frequencies							Frequencies					
	Unscaled	Scaled	Exp.[a,b,c]	I_{IR}	A_{Ra}	I_{Ra}	No	Unscaled	Scaled	Exp. [a,b,c]	I_{IR}	A_{Ra}	I_{Ra}	No	Unscaled	Scaled	Exp. [a,b,c]	I_{IR}	A_{Ra}	I_{Ra}
1	11	10		0.25	1.43	0.40	30	450	442		6.79	0.50	0.13	59	998	981	970, 967	41.60	0.10	0.00
2	16	15		0.34	2.03	0.39	31	459	451		10.90	0.66	0.16	60	1009	992		8.57	1.91	0.08
3	21	21		0.31	1.35	0.19	32	466	458	*466*	52.88	1.24	0.29	61	1030	1012		5.92	7.09	0.27
4	29	28		0.55	2.61	0.26	33	468	460		11.67	0.34	0.08	62	1053	1035		2.38	10.06	0.36
5	36	35		2.57	0.40	0.03	34	497	489	474	24.48	0.65	0.13	63	1053	1035	*1031,* 1029	7.74	2.65	0.09
6	49	48		5.81	0.64	0.04	35	513	504		4.32	0.80	0.15	64	1060	1042	1034	34.66	2.05	0.07
7	65	64		3.50	1.06	0.05	36	531	522	525	2.30	1.19	0.21	65	1076	1058	*1067*	2.61	3.93	0.13
8	71	70		2.41	1.05	0.04	37	554	544		14.12	2.06	0.33	66	1103	1084		7.19	0.77	0.02
9	95	93		5.25	1.29	0.04	38	564	554		3.04	5.24	0.81	67	1114	1095		4.47	8.79	0.27
10	104	102		3.59	0.23	0.01	39	597	586	568	9.43	4.43	0.60	68	1138	1119	1119	152.59	1.94	0.06
11	126	124		1.26	0.15	0.00	40	665	654	640, 645	16.85	1.55	0.16	69	1138	1119	*1124,* 1123	21.09	2.59	0.08
12	131	129		1.15	1.25	0.03	41	698	686		3.83	0.48	0.05	70	1169	1149		0.77	1.92	0.05
13	168	165		2.38	1.27	0.02	42	731	718	*720,* 715	7.75	5.59	0.48	71	1173	1153	1161	68.35	2.46	0.07
14	184	181		0.07	1.77	0.03	43	752	739		9.34	7.23	0.58	72	1185	1165		1.96	4.64	0.12
15	196	193		0.64	0.50	0.01	44	755	742	758	3.80	2.08	0.16	73	1202	1182	*1178,* 1174	21.43	4.52	0.12
16	206	202		1.99	0.61	0.01	45	800	786		16.54	11.85	0.82	74	1204	1184		24.40	3.78	0.10
17	219	216		0.26	0.36	0.00	46	811	798		23.38	0.36	0.02	75	1212	1191		2.83	2.30	0.06
18	224	220		0.11	0.86	0.01	47	817	803	804, *805,* 806	4.66	4.57	0.30	76	1213	1193	1204*, 1203,* 1201	11.34	10.37	0.26
19	239	235		1.65	2.90	0.03	48	839	825	*824*	1.89	4.26	0.26	77	1253	1232		27.04	1.17	0.03
20	253	249		5.15	0.95	0.01	49	845	830	841	0.88	5.74	0.35	78	1269	1247	1246, 1239	19.87	3.21	0.07
21	263	258		0.03	0.51	0.01	50	875	860		1.04	7.16	0.40	79	1271	1250		56.74	1.13	0.02
22	283	278		39.01	1.01	0.01	51	888	873		2.08	2.80	0.15	80	1282	1260	1258	75.69	1.76	0.04
23	286	281		9.92	1.19	0.01	52	900	885	*874,* 879	20.40	1.21	0.06	81	1299	1276	*1265*	41.84	13.28	0.28
24	301	296		53.83	0.98	0.59	53	919	904	896	4.35	0.25	0.01	82	1303	1281	1279	123.77	10.77	0.22
25	326	321		0.89	1.10	0.56	54	930	914		0.05	1.53	0.07	83	1307	1285	*1284,* 1282	46.61	10.75	0.22
26	364	358	*352*	2.72	2.40	0.96	55	946	930		4.05	4.27	0.20	84	1323	1300		1.44	21.31	0.42
27	369	363		0.60	1.70	0.66	56	953	937	*940,* 937, 938	1.22	8.93	0.40	85	1336	1313		10.13	1.19	0.02
28	373	367	*370*	3.45	1.93	0.73	57	961	944		0.30	4.17	0.19	86	1338	1315		0.65	2.56	0.05
29	391	384		17.20	2.90	1.00	58	989	973		0.11	0.56	0.02	87	1339	1316		1.58	9.11	0.18
88	1360	1337		2.15	3.77	0.07	106	1505	1480		6.11	1.99	0.03	124	3038	2910		21.15	81.59	0.12
89	1360	1337		1.76	4.17	0.08	107	1506	1480		38.50	2.00	0.03	125	3056	2927	2926, 2927	37.37	136.08	0.20
90	1383	1360	1348, 1346	10.99	1.63	0.03	108	1509	1484		9.83	1.48	0.02	126	3065	2936	2936	60.13	5.58	0.01
91	1389	1366		45.58	14.21	0.25	109	1535	1509	1514, 1513	197.54	2.73	0.04	127	3071	2942		35.14	44.50	0.06
92	1391	1367	*1359*	34.09	14.79	0.26	110	1553	1527	1557, 1553	140.52	1.80	0.02	128	3073	2944		1.34	12.67	0.02
93	1395	1371		6.12	0.36	0.01	111	1635	1608	1596	51.53	31.85	0.36	129	3079	2950	2948	62.44	151.93	0.22
94	1402	1378		1.12	1.91	0.03	112	1643	1615		4.94	26.03	0.29	130	3089	2959	2954	28.06	67.01	0.09
95	1417	1393	*1423,* 1419	2.64	1.26	0.02	113	1723	1651	1626, *1612*	0.75	84.13	0.81	131	3092	2962		15.80	79.39	0.11
96	1455	1430	1429	29.44	2.51	0.04	114	1727	1654	*1666,* 1639,1651	216.65	8.05	0.08	132	3095	2965		32.36	89.69	0.13
97	1475	1450	1451	16.29	10.05	0.15	115	2987	2862	2860, 2857	27.40	142.77	0.23	133	3100	2970	2970	12.95	51.14	0.07
98	1480	1455		9.81	12.54	0.18	116	3003	2877		13.14	136.29	0.22	134	3103	2973		54.63	32.15	0.04
99	1481	1456		1.54	8.64	0.13	117	3008	2882		8.12	103.69	0.16	135	3109	2978	2987	3.01	50.74	0.07
100	1485	1460	1458	4.81	3.67	0.05	118	3011	2884		38.77	163.00	0.25	136	3135	3004		20.68	101.03	0.13
101	1487	1462	*1461*	0.75	13.71	0.20	119	3014	2888		30.22	26.19	0.04	137	3145	3013	3013	17.47	93.89	0.12
102	1488	1463		1.51	5.72	0.08	120	3016	2890		33.41	39.49	0.06	138	3168	3035	3028	13.85	145.51	0.19
103	1489	1463		3.82	0.06	0.00	121	3019	2892		35.62	291.60	0.45	139	3205	3070	3073	2.94	33.50	0.04
104	1494	1469		10.46	9.91	0.14	122	3027	2900	2899	17.06	94.07	0.14	140	3625	3472	3315, 3309	15.17	55.84	0.04
105	1501	1476		10.55	12.91	0.18	123	3033	2906		19.32	200.54	0.30	141	3836	3675	3620	68.91	132.77	0.07

IIR &IRa: IR & Raman Intensities, ARa: Raman Activities, Scaling factors; 0,983 (<1700 cm-1) and 0,958 (>1700 cm-1) a El Kaaby Ekhlas A.; et al., 2016, b Sherin Percy Prema Leela et al., 2015, c Tian et al., 2018.

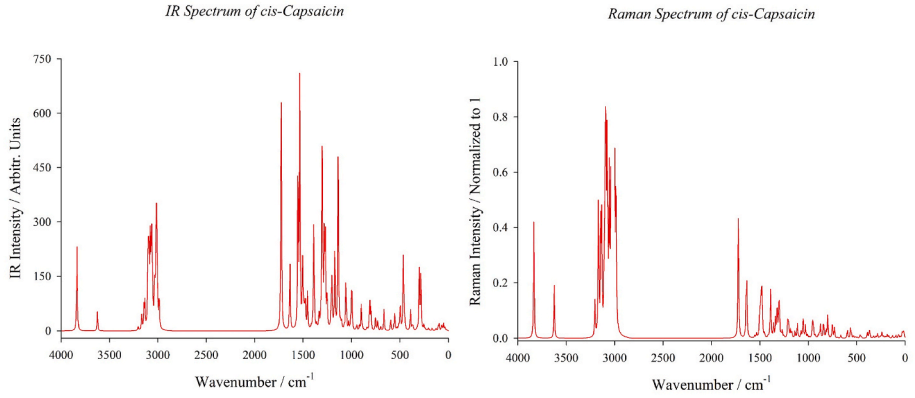

Fig. 3. The IR and Raman spectra of *cis*-Capsaicin.

frequencies for capsaicin were evaluated based on the computational results and the data mentioned above and are given below.

Although they remain in a very narrow region in the vibrational spectrum (above 3000 cm^{-1}), the absorption bands resulting from O–H–N–H and C–H stretching give information about important details of the structure. The O–H stretching is characterized by a very narrow band that appears around 3400-3600 cm^{-1}. Hydrogen bonds in the condensed phase further complicate the vibrational spectrum; hence, this band is usually either recorded as a very weak band or not observed in the spectrum. While this band is observed in the FT-IR spectrum at 3620 cm^{-1}, the 3675 cm^{-1} frequency obtained in the calculations is assigned as O–H stretching. The peak calculated at 3472 cm^{-1} and assigned as the N–H stretching was experimentally recorded at 3315 and 3309 cm^{-1} in FT-IR. A characteristic band is observed in the 1700–1800 cm^{-1} region due to the C═O stretching. The C═O double bond stretching for capsaicin was recorded at 1633 and 1651 cm^{-1} in the FT-IR and 1666 cm^{-1} in the Raman spectrum. Calculations show that this vibration mode is obtained at 1654 cm^{-1}. The pure mode calculated at 1651 cm^{-1} was determined as $C_{10} = C_{12}$ double bond stretching, and the peak at 1626 cm^{-1} obtained in the FT-IR spectrum (1612 cm^{-1} in Raman) is thought to correspond to this vibration mode. In heteroaromatic structures, CH stretching vibrations characteristically show their presence in the region of 3000–3100 cm^{-1} (Silverstein and Bassler, 1962), and the bands observed in the spectrum are not significantly affected by the nature of the substituents. The vibration modes calculated at the specified region and 3013, 3035, and 3070 cm^{-1} are due to the ring CH stretching. Vibrations numbered 115–136 are assigned as CH stretching modes of the chain. In-plane CH bending is generally observed at 1000-1300 cm^{-1}, while a lower region, 750-1000 cm^{-1}, is where out-of-plane CH bending is observed (Cinar et al., 2014). The vibrations of the ring CH bending, accompanied by CH in-plane and out-of-plane bending in the chain, were obtained in the specified regions. For example, aromatic ring CH in-plane bending at 1313 cm^{-1} and out-of-plane bending at 904 and 885 cm^{-1} are almost pure vibrational modes. As with other skeletal vibrations, the CC stretching corresponds to an absorbed band in the 1400-1600 cm^{-1} region (Silverstein and Bassler, 1962). The computed wavenumbers at 1527, 1608, and 1615 cm^{-1} correspond to the CC stretching modes of the ring, accompanied by an IR peak recorded at 1553 and 1557 cm^{-1}. It is seen that 1281 cm^{-1} (1279 cm^{-1} in IR) is the "ring breathing" mode of the aromatic ring. In the lower spectral region, the out-of-plane ring CC deformations were observed as pure or mixed modes. Vibration 109 was found at 1509 cm^{-1} and matches 1513 and 1514 cm^{-1} in the IR spectrum. This peak is assigned as pure NH in-plane bending. The 83–108 vibrations cover a region assigned as CH in-plane bending (e.g., scissoring, wagging), including methyl groups attached to the C_9 atom and the methoxy substituent. The low region of the vibrational spectrum (<600 cm^{-1}) is complex and challenging to interpret, where out-of-plane bending is observed, and modes can no longer be obtained purely. For instance, the out-of-plane bending of NH observed at 458 cm^{-1} and OH at 278 cm^{-1} was contaminated with other modes. Similarly, vibrations 17 and 18 are caused by the torsion of the methyl groups, while vibration number 14 comes from this vibration belonging to the methoxy group.

3.3. Nuclear magnetic resonance (NMR) analysis

The GIAO (Gauge Invariant Atomic Orbital) method, in which an exponential term containing the vector potential is included in each atomic orbital, is a standard method to calculate NMR spectra. In this study, proton (^1H) and carbon (^{13}C) NMR chemical shifts of capsaicin molecule were calculated in the gas phase, in chloroform and DMSO (dimethyl sulfoxide) solvents, using the GIAO method at the B3LYP/6–311++G (d, p) level. These calculated data are presented in Table 3 for *cis*-capsaicin compared with experimental NMR data recorded in $CDCl_3$ solvent and reported by Lin et al. (1993). The data for *trans*-capsaicin are given as supplementary data in Table S3. A quick look at Table 3 shows that all the calculated values for carbon chemical shifts are larger than the experimental data. Here it should be remembered once again that the observed values are recorded in the solvent and the presence of solute-solvent interactions as well as intermolecular interactions, whereas the calculations are performed for a single molecule, and the results are obtained according to the optimized structure. This can be seen from the fact that DFT calculates different values for each hydrogen atom, despite the experimental values that all hydrogens attached to the same carbon atom show the same chemical shift. The paramagnetic contribution to the shielding computed with DFT tends to be overestimated. Therefore, multiplying the calculated values with a scaling factor will bring the results closer to the experimental ones, as done for vibrational frequencies. For this study, two appropriate scaling factors were found to be 0.59 for <50 ppm and 0.89 > 50 ppm values for the ^{13}C NMR results. However, since hydrogen atoms play the most crucial role in intermolecular and solute-solvent interactions, neglecting these effects in calculating chemical shifts for each hydrogen will cause the difference to be much larger. Thus, it isn't easy to specify a similar scaling factor for proton NMR.

It is known that aromatic carbons give signals in the NMR spectrum with chemical shift values from 100 to 150 ppm (Kalinowski et al., 1988; Pihlaja and Kleinpeter, 1994). The aromatic ring C chemical shifts correspond to the experimentally specified range of 111–147 ppm, but this region should be 134–163 ppm by calculation. Since the C_5–C_8 atoms in the tail bond with two hydrogens and two carbons, their chemical shifts were obtained at low values (high region), as expected. A similar situation applies to the C_9 atom to which two methyl groups are attached. When looking at the C_{13}, a relatively higher value was recorded and estimated than the others since it also bonds with the electronegative N atom. On the other hand, methyl group C atoms have the

Table 3
Predicted ^{13}C and ^{1}H NMR isotropic chemical shifts (with respect to TMS, all values in ppm) for *cis*-Capsaicin in comparison with experimental data.

Atom	^{13}C NMR				^{1}H NMR				
	Exp. [a]	Gas	Chloroform	DMSO	Atom	Exp.[a]	Gas	Chloroform	DMSO
C(5)	26.92	46.17	46.66	47.07	H(23)	1.34	1.48	1.52	1.54
C(6)	25.37	45.44	45.30	45.19	H(24)	1.34	1.10	0.95	0.82
C(7)	29.46	52.38	52.38	52.29	H(25)	1.64	1.39	1.55	1.65
C(8)	36.55	53.76	54.59	55.06	H(26)	1.64	1.86	1.91	1.94
C(9)	26.34	52.29	52.35	52.38	H(27)	2.02	1.81	1.86	1.90
C(10)	126.58	149.60	150.76	151.37	H(28)	2.02	2.28	2.29	2.31
C(11)	172.88	189.99	193.03	194.42	H(29)	2.19	2.69	2.87	2.98
C(12)	137.82	161.04	161.13	161.23	H(30)	2.19	2.46	2.39	2.33
C(13)	43.33	58.97	59.02	59.04	H(31)	2.54	2.48	2.54	2.57
C(14)	130.07	153.43	154.33	154.87	H(32)	5.16	5.98	6.06	6.11
C(15)	23.10	37.78	37.87	37.83	H(33)	5.16	5.71	5.77	5.82
C(16)	23.10	38.19	38.16	38.11	H(34)	4.30	3.76	3.95	4.07
C(17)	110.61	133.71	133.87	133.69	H(35)	4.30	5.27	5.19	5.14
C(18)	120.52	137.16	138.64	139.81	H(36)	6.07	6.08	6.54	6.78
C(19)	146.69	163.96	163.57	163.08	H(37)	0.90	1.49	1.51	1.53
C(20)	114.35	133.57	134.85	135.77	H(38)	0.90	1.43	1.38	1.37
C(21)	145.03	159.76	159.52	159.25	H(39)	0.90	1.14	1.18	1.23
C(22)	55.76	69.33	70.01	70.34	H(40)	0.90	1.21	1.22	1.26
					H(41)	0.90	1.49	1.50	1.53
					H(42)	0.90	1.64	1.51	1.36
					H(43)	6.76	8.29	8.30	8.29
					H(44)	6.69	6.97	7.18	7.33
					H(45)	6.81	7.05	7.32	7.48
					H(46)	6.17	4.25	4.84	5.13
					H(47)	3.80	4.55	4.62	4.65
					H(48)	3.80	4.01	4.11	4.17
					H(49)	3.80	4.22	4.26	4.25

Predicted average chemical shifts for TMS; H: 32,36 ppm and C: 195.5 (Gas), 195,9 (Chloroform), 196,1 (DMSO) ppm.
[a] Lin et al. (1993).

lowest chemical shift values, as expected. Due to its bond with another electronegative atom, O, the C_{22} has the highest chemical shift value among the atoms mentioned above. The chemical shift value of C_{11}, which bonds with O and N, gave the enormous value (low region) - estimated at around 190 ppm, recorded at about 173 ppm. While the C_{10} and C_{12} atoms, linked to each other by double bonds, gave signals at 127 and 138 ppm, the calculations were approximately 25 ppm and 15 ppm larger for these atoms, respectively.

It is seen that there is a linear correlation between the chemical shift values calculated by DFT and experimentally recorded. The relationship equations obtained for the recorded and calculated proton and carbon chemical shifts for the chloroform solvent are given below.

$$^{13}C: \delta_{cal} = 1.0055\delta_{exp} + 18.549 \ (R^2 = 0.9953)$$

$$^{1}H: \delta_{cal} = 1.033\delta_{exp} + 0.2371 \ (R^2 = 0.9455)$$

Figs. S2a and b (in supplementary material) show correlation graphs of carbon and proton chemical shift values for all three media (gas phase, chloroform and DMSO solvent), respectively.

3.4. Electronic feature analysis

To understand the electronic transitions of the studied molecule, TD-DFT calculations were made on the electronic absorption spectrum by considering the three lowest singlets → singlet spin-allowed excited states in a vacuum and ethanol solvent. The simulated UV spectra of *cis*-capsaicin are given in Fig. 4, and the calculated excitation energies, oscillator strength (f), absorption wavelength (λ), and spectral excitations are presented in Table 4. Recently, the UV–Vis spectrum of capsaicin was recorded by Qais et al. (2017), and an absorption peak at 280 nm was obtained. However, theoretical calculations found this peak at 264 nm for the gas phase and 259 nm in ethanol solvent. This electronic absorption corresponds to the transition from ground to the first excited state and is characterized by an electron excitation from the HOMO to the LUMO and assigned as π→π*.

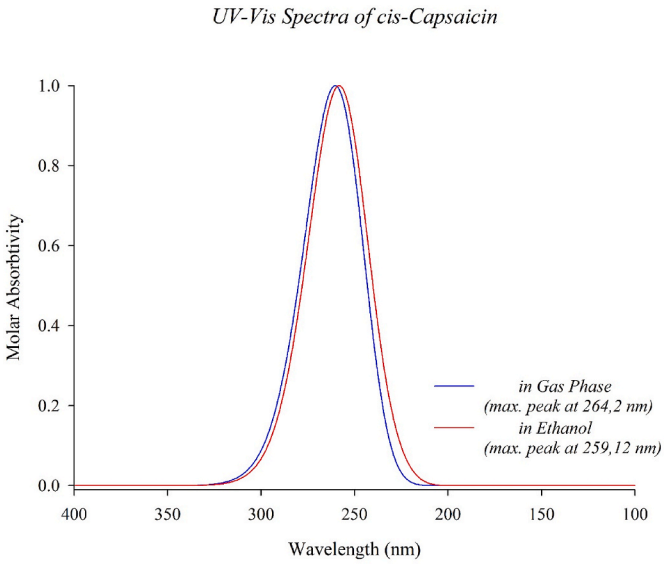

Fig. 4. The UV–Vis spectra of *cis*-Capsaicin in gas phase and in ethanol solution.

Table 4
The calculated absorption wavelength, λ (nm), excitation energies E (eV) and oscillator strengths (f) of *cis*-Capsaicin obtained at TD-DFT (B3LYP/6–311++G (d,p).

Gas			*Ethanol*		
λ (nm)	*E (eV)*	*f*	*λ (nm)*	*E (eV)*	*f*
264.20	4.6928	0.0125	259.12	4.7848	0.0816
259.66	4.7749	0.0496	250.65	4.9464	0.0008
251.20	4.9357	0.0017	237.48	5.2208	0.0088

Molecular orbitals and their properties, such as energy, are essential parameters for quantum chemistry. HOMO and LUMO are frontier orbitals involved in chemical stability (Gunasekarana et al., 2008). HOMO represents the ability to donate an electron, while LUMO, an electron acceptor, represents the ability to gain an electron. Molecular orbitals are also used by frontier electron density to estimate the most reactive position in π-electron systems and explain various reactions in conjugated systems (Fukui et al., 1952). The slight difference between the energies of the LUMO and HOMO is used to characterize conjugated molecules. This results from significant intramolecular charge transfer from the end-capping electron donor groups to the efficient electron acceptor groups via the π-conjugate pathway. The energy of HOMO is directly related to the ionization potential, while the energy of LUMO is related to electron affinity. The energy difference between the HOMO and the LUMO orbital is called the energy gap, which is important stability for structures (Ravikumar et al., 2008). Once the HOMO and LUMO energy values of a molecule or molecular system are obtained, these values can be used to compute the other essential parameters such as ionization potential, electron affinity, chemical hardness and softness, electronegativity, electronic chemical potential, and electrophilic index which is expressed as the tendency of a molecule as a whole to accommodate electrons. These terms can be used to analyze a substance's structure, characteristics, reactivity, dynamics, toxicity, aromaticity, and other factors. Using the total energy and Koopmans theorem, the ionization potential and electron affinity, which describe the electrical properties of molecules, can be calculated as $I = -E_{HOMO}$ and $A = -E_{LUMO}$, respectively (Bilkan, 2019). Some important properties calculation such as chemical potential, chemical hardness and electrophilicity are explained by Parr (Parr et al., 1999). In addition to the HOMO and LUMO energy levels, the other mentioned parameters which give information about the electronic and chemical features of the steady molecule were calculated and tabulated in Table 5. From the TD-DFT calculations, the HOMO and LUMO energies of cis-capsaicin and the energy difference between these two levels were obtained as −5.86 eV, −0.51 eV, and 5.35 eV, respectively. The plots of these important orbitals are shown in Fig. 5. Electron affinity (A) is a quantity that can be measured experimentally and physically observed, and is equal to the difference in energy of a neutral atom and its gaseous anion. Electronegativity (χ) and electrophilicity (ψ) are other arbitrarily defined chemical concepts associated with electron affinity. Electronegativity, on the other hand, can be defined as the power of an atom to attract electrons and was formulated by Mulliken (1934) as half the sum of the ionization potential and electron affinity. Thus, large values of I and A in a system mean that the system will choose to accept electrons rather than lose electrons. This value for the examined compound was found as 3.1871 eV. The measure of a system's reactivity to attract electrons from a nucleophile to form a bond is defined as electrophilicity and is directly proportional to chemical potential, which is the negative of electronegativity, and inversely proportional to chemical hardness (η) (see Table 5). For the concept in question, a value of 1.8986 was obtained in this study. The A and χ values for capsaicin are positive, suggesting that it no longer prefers to reject electrons as electron-nuclear attraction overtakes electron-electron repulsion.

Table 5
The HOMO&LUMO energies and computed other parameters of *cis*-Capsaicin.

Parameters	Formula	Results
LUMO energy (eV)	E_{LUMO}	−0.51212
HOMO energy (eV)	E_{HOMO}	−5.86215
Energy band gap	$\Delta E = E_{LUMO} - E_{HOMO}$	5.3500
Ionization potential	$I = -E_{HOMO}$	5.8622
Electron affinity	$A = -E_{LUMO}$	0.5121
Chemical hardness	$\eta = (I - A)/2$	2.6750
Chemical softness	$\xi = 1/2\eta$	0.1869
Electronegativity	$\chi = (I + A)/2$	3.1871
Chemical potential	$\mu = -(I + A)/2$	−3.1871
Electrophilicity index	$\psi = \mu^2/2\eta$	1.8986

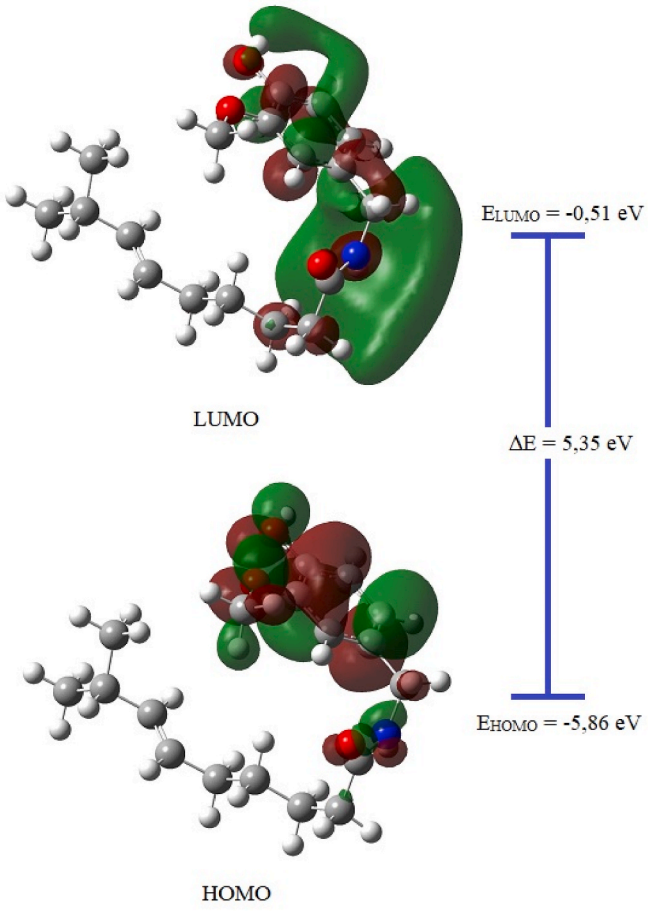

Fig. 5. The LUMO & HOMO molecular orbitals and energies of *cis*-Capsaicin.

Mulliken Population Analysis is often used to calculate a qualitative estimate of the partial atomic charges of a molecule because it measures how the electronic structure changes under atomic displacement. Many properties of a molecule, such as a dipole moment, polarizability, electronic structure etc., can be determined by Mulliken charge. In order to determine atomic charges and orbital populations of molecular wave functions in generic atomic orbital basis sets, a technique known as "natural population analysis" has been devised. The natural analysis is an alternative to the more used Mulliken population analysis, and it appears to have superior numerical stability and a better capacity to characterize the distribution of electrons in compounds with strong ionicity (Bilkan et al., 2016), like those containing metal atoms. Table 6 shows the predicted atomic charges obtained with the Mulliken and Natural Population Analysis for each atom, while Fig. S3 (in supplementary materials) shows it schematically. As expected, the total charge is equal to zero. Table 6 shows that the atomic charges obtained with Natural Population Analysis (NPA) are generally larger than those obtained with Mulliken Analysis. NPA gave positive results for the atomic charges of C(11), C(19) and C(21) for non-hydrogen atoms. Considering that all three of these atoms are bound to electronegative Oxygen atoms, the results are quite plausible. Milliken Analysis, on the other hand, predicted the atomic charge of C(9), C(10), C(20), and C(21) as positive, while giving a negative value for H(24), unlike NPA, which says that all hydrogen atoms have positive charges.

The Hirshfeld surface is defined as the area occupied by a molecule in a crystal by dividing the crystal electron density into molecular parts (Spackman and Byrom, 1997; Spackman and Jayatilaka, 2009), and by scanning the van der Waals distances and identifying the interaction sites, the Hirshfeld surface for a molecule is obtained (Hirshfeld, 1977).

Table 6
The atomic charges obtained by Mulliken and Natural Population Analysis.

Atom	Mulliken	Natural	Atom	Mulliken	Natural
O(1)	−0.386	−0.649	H(23)	0.187	0.227
O(2)	−0.287	−0.524	H(24)	−0.031	0.235
O(3)	−0.494	−0.690	H(25)	0.151	0.217
N(4)	−0.160	−0.667	H(26)	0.156	0.233
C(5)	−0.126	−0.450	H(27)	0.173	0.229
C(6)	−0.356	−0.441	H(28)	0.150	0.230
C(7)	−0.696	−0.471	H(29)	0.170	0.243
C(8)	−0.190	−0.525	H(30)	0.159	0.258
C(9)	0.491	−0.301	H(31)	0.167	0.231
C(10)	0.515	−0.216	H(32)	0.143	0.217
C(11)	−0.328	0.684	H(33)	0.128	0.216
C(12)	−0.587	−0.204	H(34)	0.155	0.234
C(13)	−0.287	−0.266	H(35)	0.189	0.263
C(14)	0.188	−0.073	H(36)	0.317	0.417
C(15)	−0.653	−0.648	H(37)	0.160	0.226
C(16)	−0.634	−0.647	H(38)	0.164	0.230
C(17)	−0.012	−0.299	H(39)	0.155	0.221
C(18)	−0.303	−0.245	H(40)	0.160	0.224
C(19)	−0.311	0.286	H(41)	0.160	0.225
C(20)	0.203	−0.303	H(42)	0.129	0.233
C(21)	0.144	0.277	H(43)	0.179	0.261
C(22)	−0.110	−0.296	H(44)	0.089	0.233
			H(45)	0.100	0.231
			H(46)	0.381	0.500
			H(47)	0.154	0.223
			H(48)	0.157	0.203
			H(49)	0.175	0.204

Once the Hirshfeld surface is obtained, the parameters d_e and d_i are also determined, corresponding to the distance from the Hirshfeld surface to the nearest outer core and the distance to the nearest core on the surface, respectively. The d_{norm} represents the normalized contact distance that allows the identification of regions that are particularly important for intermolecular interactions and is obtained by the following formula, depending on the d_e, d_i and radii of the atom νdw (Spackman and McKinnon, 2002);

$$d_{norm} = \frac{d_i - r_i^{\nu dw}}{r_i^{\nu dw}} + \frac{d_e - r_e^{\nu dw}}{r_e^{\nu dw}}$$

Fig. 6 (top) shows the 3D Hirshfeld surface of capsaicin obtained and mapped over d_{norm}. Here, bright red dots on the Hirshfeld surface indicate OH interactions, and light red dots indicate CH···O interactions. Other visible points represent the H···H contacts on the surface. A 2D fingerprint plot of the surfaces with the partial contribution of the entire surface is presented in Fig. 6 (bottom) to highlight the close contacts of specific atom pairs such as H–H, O–H/H–O, and C–H/H–C. If $d_e < d_i$, the molecule is said to be an acceptor, and if $d_e > d_i$, the molecule is said to be a donor, this is observed as complementary regions in the fingerprint graph.

The two sharp spikes in the 2D fingerprint plots show the typical O–H···O interaction. The contribution of this interaction to the total surface is 15.7%. Indicative of C–H···π interactions are prominent "wings," which are visible in Fig. 6. The contribution of C–H···C interactions to the total surface was determined as 15.2%. The total contribution of the H–H interactions, seen as the most dominant interaction, was calculated as 67.2% and thus covered most of the Hirshfeld surface. Since the contribution of interactions originating from the nitrogen atom is negligible, it is not shown here.

The Molecular Electrostatic Potential (MESP) map is another important tool often used to study intermolecular interactions in a molecular system and identify nucleophilic and electrophilic attack localizations. In these maps, a color scale from red to dark blue is used to characterize the structure's extremely negative and positive regions under consideration. For example, yellow represents a less negative, and light blue corresponds to a less positive region. Regions that can be considered approximately as the neutral zone are shown in green. In the map given in Fig. 7, it is seen that prominent colors in the form of yellow-orange are located around the Oxygen atoms. These regions show O–H···O interactions and are electronegatively labeled concerning the Hirshfeld surface. The absence of dark blue regions on the map indicates the structure's lack of highly positive regions.

As it is known, the number of occupied states per unit volume at a specific energy of a system that has reached thermal equilibrium value

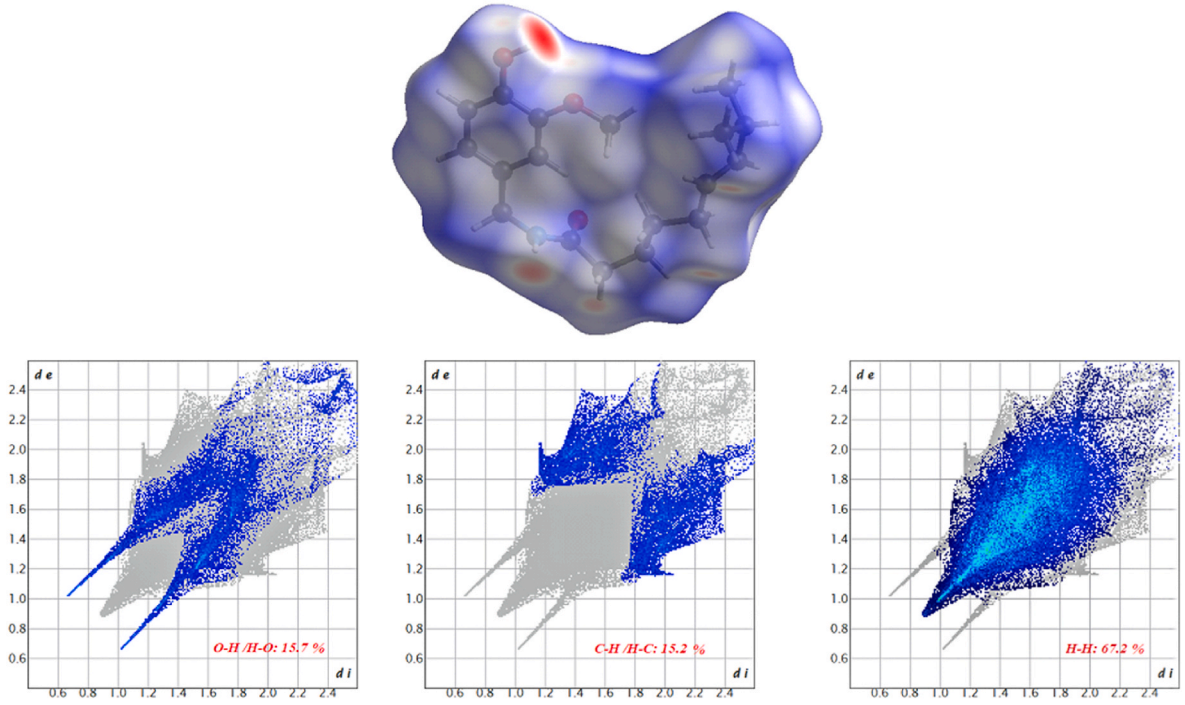

Fig. 6. The Hirshfeld surface (top) and the 2D fingerprint histogram resolved into O···H, C···H and H···H contacts (bottom).

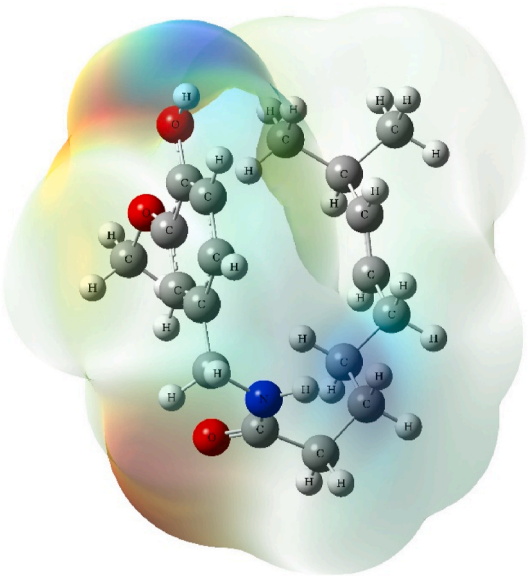

Fig. 7. The molecular electronic potential (MEP) surfaces.

indicates the DOS (Density of States). The DOS plays a critical role in the kinetic theory of materials. Therefore, in this study, the DOS and PDOS spectra of capsaicin under investigation were examined and are present in Fig. 8. The chemical structure of capsaicin consists of three critical regions: A (Aromatic head), B (Amide group) and C (Hydrophobic tail). As seen in Fig. 8, DOS spectra were drawn considering these three critical regions. In this graph, the minimum of the conduction band corresponds to the value at which the binding energy is zero (E = 0). The valance and conduction bands are dominated by the contributions of the hydrophobic tail of capsaicin. However, the contributions of other regions are too significant to be ignored. The contributions of the specified

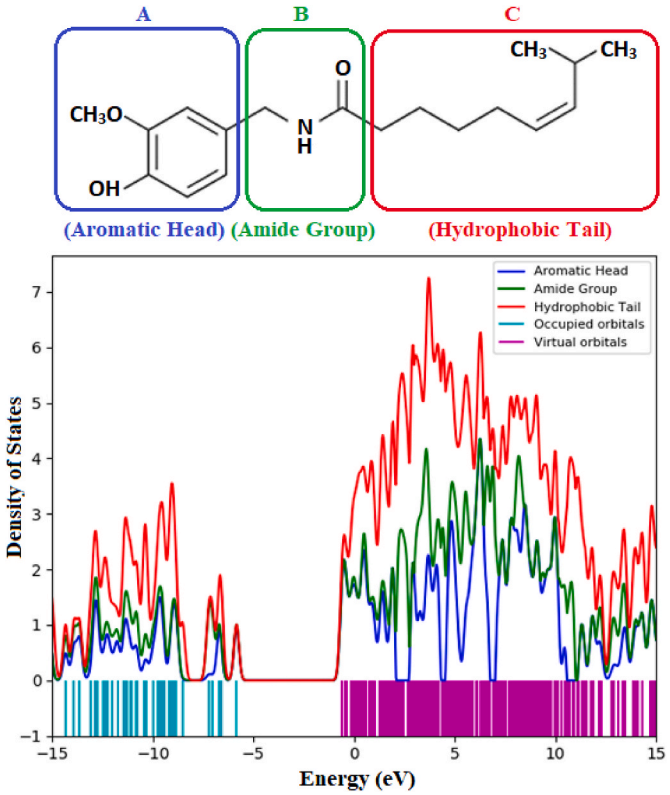

Fig. 8. The DOS and PDOS spectra of *cis*-Capsaicin.

regions of capsaicin to the DOS levels are C, B and A, respectively. The lowest contribution is from the A region because the number of H-bonding in this region is high. Moreover, the contributions of the 2p orbitals of the $_6$C, $_7$N and $_8$O elements in capsaicin structure are more dominant in the valence and conduction bands. Furthermore, the energy band gap value between the top of the valence band and the bottom of the conduction band was observed as about 5.35 eV. This value was determined to be equivalent to the energy difference between HOMO and LUMO levels of cis-capsaicin (see Fig. 5).

4. Conclusion

In this study, the molecular structure, spectroscopic properties and DOS levels of capsaicin were comprehensively determined using DFT and presented by comparing them with experimental data. It was determined that there is a perfect agreement between the data obtained as a result of our optimization studies for the molecule isolated under vacuum conditions and the experimental data in the literature. A highly concordant correlation (R^2 = 0.99325) was obtained between the calculated bond lengths and the x-ray crystallographic data. Moreover, a good match was observed between the corresponding experimental results and the data obtained for bond angles (except for the angles where N and O atoms are located). The most significant difference was observed for the O1=C11–C8 bond angle by calculating 6.4° larger. Contrary to these good harmonies, some deviations according to experimental data recorded in the literature were seen in dihedral angles arising from intermolecular interactions. The relationships for chemical shifts of carbon and hydrogen atoms by evaluating the experimental data according to the calculations made in chloroform solvent were found as $1.0055\delta_{exp}$ +18.549 and $1.033\delta_{exp}$ +0.2371, respectively. It was determined by TDDFT calculations that the UV–Vis radiation for the studied molecule is absorbed at 264 nm and 259 nm for the gas phase and ethanol solvent, respectively. These absorption peaks were assigned as π−π* electronic transitions between LUMO and HOMO energy levels (energy gap is 5.35 eV), and the other essential parameters were calculated as follows: electron affinity at 0.512, chemical hardness at 2.675, chemical softness at 0.187, electronegativity at 3.187 and electrophilicity index at 1.899. From Hirshfeld surface analysis, the contribution of O–H···O and C–H···C interactions to the total surface was computed as 15.7% and 15.2%, respectively. The total contribution of the H–H interactions, seen as the most dominant interaction, was calculated as 67.2% and determined to cover most of the Hirshfeld surface. Lastly, from the DOS spectra analysis, it was determined that the contributions of the regions of capsaicin to the DOS levels are C (Hydrophobic tail), B (Amide group) and A (Aromatic head), respectively.

Author statement

Mehmet ÇINAR: Review & Editing, Software, Visualization, Writing, Project administration. **Bünyamin ALIM:** Writing, Review & Editing, Software, Conceptualization, Original draft. **Zuhal ALIM:** Review & Editing, Investigation, Data Curation. **Erdem ŞAKAR:** Writing, Review & Editing.

Declaration of competing interest

The authors declare that they have no known competing financial interests or personal relationships that could have appeared to influence the work reported in this paper.

Data availability

No data was used for the research described in the article.

Appendix A. Supplementary data

Supplementary data to this article can be found online at https://doi.org/10.1016/j.radphyschem.2023.110879.

References

Abdel-Salam, O.M.E., 2014. Capsaicin as a therapeutic molecule. In: Abdel-Salam, O.M.E. (Ed.), Progress in drug research. Fortschritte der Arzneimittelforschung. Progres des recherches pharmaceutiques, vol. 68. Springer Science & Business Media.

Adamo, C., Scuseria, G.E., Barone, V., 1999. Accurate excitation energies from time-dependent density functional theory: assessing the PBE0 model. J. Chem. Phys. 111 (7), 2889. https://doi.org/10.1063/1.479571.

Agrawal, R.C., Wiessler, M., Hecker, E., Bhide, S.V., 1986. Tumour-promoting effect of chilli extract in BALB/c mice. Int. J. Cancer 38 (5), 689–695. https://doi.org/10.1002/IJC.2910380512.

Athanasiou, A., Smith, P.A., Vakilpour, S., Kumaran, N.M., Turner, A.E., Bagiokou, D., Layfield, R., Ray, D.E., Westwell, A.D., Alexander, S.P.H., Kendall, D.A., Lobo, D.N., Watson, S.A., Lophatanon, A., Muir, K.A., Guo, D. an, Bates, T.E., 2007. Vanilloid receptor agonists and antagonists are mitochondrial inhibitors: how vanilloids cause non-vanilloid receptor mediated cell death. Biochem. Biophys. Res. Commun. 354 (1), 50–55. https://doi.org/10.1016/J.BBRC.2006.12.179.

Bauernschmitt, R., Ahlrichs, R., 1996. Treatment of electronic excitations within the adiabatic approximation of time dependent density functional theory. Chem. Phys. Lett. 256 (4–5), 454–464. https://doi.org/10.1016/0009-2614(96)00440-X.

Becke, A.D., 1998. Density-functional thermochemistry. I. The effect of the exchange-only gradient correction. J. Chem. Phys. 96 (3), 2155. https://doi.org/10.1063/1.462066.

Bilkan, M.T., 2019. Quantum chemical studies on solvent effects, ligand–water complexes and dimer structure of 2,2'-dipyridylamine. Phys. Chem. Liq. 57 (1), 100–116. https://doi.org/10.1080/00319104.2018.1423564.

Bilkan, M.T., Yurdakul, Ş., Demircioglu, Z., Buyukgungor, O., 2016. Crystal structure, FT-IR, FT-Raman and DFT studies on a novel compound [C10H9N3]4AgNO3. J. Organomet. Chem. 805, 108–116. https://doi.org/10.1016/j.jorganchem.2016.01.014.

Bley, K., Boorman, G., Mohammad, B., McKenzie, D., Babbar, S., 2012. A comprehensive review of the carcinogenic and anticarcinogenic potential of capsaicin. Toxicol. Pathol. 40 (6), 847–873. https://doi.org/10.1177/0192623312444471.

Bora, P.K., Kemprai, P., Barman, R., Das, D., Nazir, A., Saikia, S.P., Banik, D., Haldar, S., 2021. A sensitive 1H NMR spectroscopic method for the quantification of capsaicin and capsaicinoid: morpho-chemical characterisation of chili land races from northeast India. Phytochem. Anal. 32 (1), 91–103. https://doi.org/10.1002/PCA.2934.

Brederson, J.D., Kym, P.R., Szallasi, A., 2013. Targeting TRP channels for pain relief. Eur. J. Pharmacol. 716 (1–3), 61–76. https://doi.org/10.1016/J.EJPHAR.2013.03.003.

Casida, M.E., Jamorski, C., Casida, K.C., Salahub, D.R., 1998. Molecular excitation energies to high-lying bound states from time-dependent density-functional response theory: characterization and correction of the time-dependent local density approximation ionization threshold. J. Chem. Phys. 108 (11), 4439. https://doi.org/10.1063/1.475855.

Chong, D.P., 1995. In: Chong, D.P. (Ed.), Recent Advances in Density Functional Methods, vol. 1. WORLD SCIENTIFIC. https://doi.org/10.1142/2914.

Cinar, M., Coruh, A., Karabacak, M., 2011. FT-IR, UV–vis, 1H and 13C NMR spectra and the equilibrium structure of organic dye molecule disperse red 1 acrylate: a combined experimental and theoretical analysis. Spectrochim. Acta Mol. Biomol. Spectrosc. 83 (1), 561–569. https://doi.org/10.1016/J.SAA.2011.09.003.

Cinar, M., Coruh, A., Karabacak, M., 2014. A comparative study of selected disperse azo dye derivatives based on spectroscopic (FT-IR, NMR and UV–Vis) and nonlinear optical behaviors. Spectrochim. Acta Mol. Biomol. Spectrosc. 122, 682–689. https://doi.org/10.1016/J.SAA.2013.11.106.

David, W.I.F., Shankland, K., Shankland, N., 1998. Routine determination of molecular crystal structures from powder diffraction data. Chem. Commun. 8, 931–932. https://doi.org/10.1039/A800855H, 0.

Dltchfield, R., 2003. Molecular orbital theory of magnetic shielding and magnetic susceptibility. J. Chem. Phys. 56 (11), 5688. https://doi.org/10.1063/1.1677088.

Dreuw, A., Head-Gordon, M., 2004. Failure of time-dependent density functional theory for long-range charge-transfer excited states: the zincbacteriochlorin-bacteriochlorin and bacteriochlorophyll-spheroidene complexes. J. Am. Chem. Soc. 126 (12), 4007–4016. https://doi.org/10.1021/JA039556N/SUPPL_FILE/JA039556NSI20040114_085038.PDF.

El Kaaby Ekhlas, A., Al Hattab Zahra, N., Ai-Anny Jenan, A., 2016. FT-IR Identification of Capsaicin from callus and seedling of chilli pepper plants Capsicum annuum L. in vitro. Int. J. Med. Clin. Res. 4, 1144–1146.

Frisch, M.J., Trucks, G.W., Schlegel, H.B., Scuseria, G.E., Robb, M.A., Cheeseman, J.R., Scalmani, G., Barone, V., Petersson, G.A., Nakatsuji, H., Li, X., Caricato, M., Marenich, A., Bloino, J., Janesko, B.G., Gomperts, R., Mennucci, B., Hratchian, H.P., Ort, J.V., 2009. *Gaussian 09* (Revision A.1). Gaussian, Inc.

Fukui, K., Yonezawa, T., Shingu, H., 1952. A molecular orbital theory of reactivity in aromatic hydrocarbons. J. Chem. Phys. 20 (4), 725. https://doi.org/10.1063/1.1700523.

Galano, A., Martínez, A., 2012. Capsaicin, a tasty free radical scavenger: mechanism of action and kinetics. J. Phys. Chem. B 116 (3), 1200–1208. https://doi.org/10.1021/JP211172F/ASSET/IMAGES/JP211172F.SOCIAL.JPEG_V03.

Gunasekarana, S., Arun Balajia, R., Kumaresan, S., Anand, G., Srinivasan, S., 2008. Experimental and theoretical investigations of spectroscopic properties of N-acetyl-5-methoxytryptamine SILVER NANO PARTICLES FROM SEA WEEDS View project Spectroscopic and computational investigations on bioactive compounds extracted from medicinal plants. Can. J. Anal. Sci. Spectrosc. 53 (4), 149–162.

Hail, N., Lotan, R., 2002. Examining the role of mitochondrial respiration in vanilloid-induced apoptosis. JNCI: J. Natl. Cancer Inst. 94 (17), 1281–1292. https://doi.org/10.1093/JNCI/94.17.1281.

Hirshfeld, F.L., 1977. Bonded-atom fragments for describing molecular charge densities. Theor. Chim. Acta 44 (2), 129–138. https://doi.org/10.1007/BF00549096, 1977 44: 2.

Ito, K., Nakazato, T., Yamato, K., Miyakawa, Y., Yamada, T., Hozumi, N., Segawa, K., Ikeda, Y., Kizaki, M., 2004. Induction of apoptosis in leukemic cells by homovanillic acid derivative, capsaicin, through oxidative StressImplication of phosphorylation of p53 at ser-15 residue by reactive oxygen species. Cancer Res. 64 (3), 1071–1078. https://doi.org/10.1158/0008-5472.CAN-03-1670.

Jamorski, C., Casida, M.E., Salahub, D.R., 1998. Dynamic polarizabilities and excitation spectra from a molecular implementation of time-dependent density-functional response theory: N2 as a case study. J. Chem. Phys. 104 (13), 5134. https://doi.org/10.1063/1.471140.

Kalinowski, H.O., Berger, S., Braun, S., 1988. Carbon-13 NMR Spectroscopy.

Kang, J.H., Kim, C.S., Han, I.S., Kawada, T., Yu, R., 2007. Capsaicin, a spicy component of hot peppers, modulates adipokine gene expression and protein release from obese-mouse adipose tissues and isolated adipocytes, and suppresses the inflammatory responses of adipose tissue macrophages. FEBS (Fed. Eur. Biochem. Soc.) Lett. 581 (23), 4389–4396. https://doi.org/10.1016/J.FEBSLET.2007.07.082.

Karabacak, M., Kurt, M., Cnar, M., Coruh, A., 2009. Experimental (UV, NMR, IR and Raman) and Theoretical Spectroscopic Properties of 2-Chloro-6-Methylaniline, vol. 107, pp. 253–264. https://doi.org/10.1080/00268970902821579, 3.

Karabacak, M., Cinar, M., Kurt, M., 2010. DFT based computational study on the molecular conformation, NMR chemical shifts and vibrational transitions for N-(2-methylphenyl) methanesulfonamide and N-(3-methylphenyl) methanesulfonamide. J. Mol. Struct. 968 (1–3), 108–114. https://doi.org/10.1016/J.MOLSTRUC.2010.01.033.

Keresztury, G., 2006. Raman spectroscopy: theory. In: Chalmers, J.M., Griffith, P.R. (Eds.), Handbook of Vibrational Spectroscopy. John Wiley & Sons, Ltd. https://doi.org/10.1002/0470027320.S0109.

Keresztury, G., Holly, S., Besenyei, G., Varga, J., Wang, A., Durig, J.R., 1993. Vibrational spectra of monothiocarbamates-II. IR and Raman spectra, vibrational assignment, conformational analysis and ab initio calculations of S-methyl-N,N-dimethylthiocarbamate. Spectrochim. Acta Mol. Spectros 49 (13–14), 2007–2026. https://doi.org/10.1016/S0584-8539(09)91012-1.

Kim, C.S., Kawada, T., Kim, B.S., Han, I.S., Choe, S.Y., Kurata, T., Yu, R., 2003. Capsaicin exhibits anti-inflammatory property by inhibiting IkB-a degradation in LPS-stimulated peritoneal macrophages. Cell. Signal. 15 (3), 299–306. https://doi.org/10.1016/S0898-6568(02)00086-4.

Kurt, M., Babu, P.C., Sundaraganesan, N., Cinar, M., Karabacak, M., 2011. Molecular structure, vibrational, UV and NBO analysis of 4-chloro-7-nitrobenzofurazan by DFT calculations. Spectrochim. Acta Mol. Biomol. Spectrosc. 79 (5), 1162–1170. https://doi.org/10.1016/J.SAA.2011.04.037.

Lee, C., Yang, W., Parr, R.G., 1988. Development of the Colle-Salvetti correlation-energy formula into a functional of the electron density. Phys. Rev. B 37 (2), 785. https://doi.org/10.1103/PhysRevB.37.785.

Lee, J.S., Chang, J.S., Lee, J.Y., Kim, J.A., 2004. Capsaicin-induced apoptosis and reduced release of reactive oxygen species in MBT-2 Murine Bladder Tumor cells. Arch Pharm. Res. (Seoul) 27 (11), 1147–1153. https://doi.org/10.1007/BF02975121, 2004 27:11.

Lee, Y.S., Kang, Y.S., Lee, J.S., Nicolova, S., Kim, J.A., 2009. Involvement of NADPH Oxidase-Mediated Generation of Reactive Oxygen Species in the Apototic Cell Death by Capsaicin in HepG2 Human Hepatoma Cells, vol. 38, pp. 405–412. https://doi.org/10.1080/10715760410001665262, 4.

Lin, L.-Z., West, D.P., Cordell, G.A., 1993. NMR assignments of cis- and trans-capsaicin. Nat. Prod. Lett. 3 (1), 5–8. https://doi.org/10.1080/10575639308043831.

López-carnllo, L., Avila, M.H., Dubrow, R., 1994. Chili pepper consumption and gastric cancer in Mexico: a case-control study. Am. J. Epidemiol. 139 (3), 263–271. https://doi.org/10.1093/OXFORDJOURNALS.AJE.A116993.

Mori, A., Lehmann, S., O'Kelly, J., Kumagai, T., Desmond, J.C., Pervan, M., McBride, W.H., Kizaki, M., Koeffler, H.P., 2006. Capsaicin, a component of red peppers, inhibits the growth of androgen-independent, p53 mutant prostate cancer cells. Cancer Res. 66 (6), 3222–3229. https://doi.org/10.1158/0008-5472.CAN-05-0087.

Mulliken, R.S., 1934. A new electroaffinity scale; together with data on valence states and on valence ionization potentials and electron affinities. J. Chem. Phys. 2 (11), 782–793.

Nelson, E.K., Dawson, D.E., 1923. The constitution of capsaicin, the pungent principle of Capsicum. III. J. Am. Chem. Soc. 45 (9), 2179–2181. https://doi.org/10.1021/JA01662A023.

O'Boyle, N.M., Tenderholt, A.L., Langner, K.M., 2008. cclib: a library for package-independent computational chemistry algorithms. J. Comput. Chem. 29 (5), 839–845. https://doi.org/10.1002/JCC.20823.

Parr, R.G., Szentpály, L.V., Liu, S., 1999. Electrophilicity index. J. Am. Chem. Soc. 121 (9), 1922–1924. https://doi.org/10.1021/JA983494X.

Patowary, P., Pathak, M.P., Zaman, K., Raju, P.S., Chattopadhyay, P., 2017. Research progress of capsaicin responses to various pharmacological challenges. Biomed. Pharmacother. 96, 1501–1512. https://doi.org/10.1016/J.BIOPHA.2017.11.124.

Perdew, J.P., Wang, Y., 1992. Accurate and simple analytic representation of the electron-gas correlation energy. Phys. Rev. B 45 (23), 13244. https://doi.org/10.1103/PhysRevB.45.13244.

Petersilka, M., Gossmann, U.J., Gross, E.K.U., 1996. Excitation energies from time-dependent density-functional theory. Phys. Rev. Lett. 76 (8), 1212. https://doi.org/10.1103/PhysRevLett.76.1212.

Pihlaja, K., Kleinpeter, E., 1994. Carbon-13 NMR Chemical Shifts in Structural and Stereochemical Analysis. VCH.

Pramanik, K.C., Boreddy, S.R., Srivastava, S.K., 2011. Role of mitochondrial electron transport chain complexes in capsaicin mediated oxidative stress leading to apoptosis in pancreatic cancer cells. PLoS One 6 (5), e20151. https://doi.org/10.1371/JOURNAL.PONE.0020151.

Price, L.S., Collard, J.G., 2001. Regulation of the cytoskeleton by Rho-family GTPases: implications for tumour cell invasion. Semin. Cancer Biol. 11 (2), 167–173. https://doi.org/10.1006/SCBI.2000.0367.

Qais, F.A., Abdullah, K.M., Alam, M.M., Naseem, I., Ahmad, I., 2017. Interaction of capsaicin with calf thymus DNA: a multi-spectroscopic and molecular modelling study. Int. J. Biol. Macromol. 97, 392–402. https://doi.org/10.1016/J.IJBIOMAC.2017.01.022.

Ravikumar, C., Joe, I.H., Jayakumar, V.S., 2008. Charge transfer interactions and nonlinear optical properties of push–pull chromophore benzaldehyde phenylhydrazone: a vibrational approach. Chem. Phys. Lett. 460 (4–6), 552–558. https://doi.org/10.1016/J.CPLETT.2008.06.047.

Scott, A.P., Radom, L., 1996. Harmonic vibrational frequencies: an evaluation of Hartree-Fock, Møller-Plesset, quadratic configuration interaction, density functional theory, and semiempirical scale factors. J. Phys. Chem. 100 (41), 16502–16513. https://doi.org/10.1021/JP960976R/SUPPL_FILE/JP16502A.PDF.

Serra, I., Yamamoto, M., Calvo, A., Cavada, G., Báez, S., Endoh, K., Watanabe, H., Tajima, K., 2002. Association of chili pepper consumption, low socioeconomic status and longstanding gallstones with gallbladder cancer in a Chilean population. Int. J. Cancer 102 (4), 407–411. https://doi.org/10.1002/IJC.10716.

Sherin Percy Prema Leela, J., Hemamalini, R., Muthu, S., Al-Saadi, A.A., 2015. Spectroscopic investigation (FTIR spectrum), NBO, HOMO–LUMO energies, NLO and thermodynamic properties of 8-Methyl-N-vanillyl-6-nonenamideby DFT methods. Spectrochim. Acta Mol. Biomol. Spectrosc. 146, 177–186. https://doi.org/10.1016/J.SAA.2015.03.027.

Shin, D.H., Kim, O.H., Jun, H.S., Kang, M.K., 2008. Inhibitory effect of capsaicin on B16-F10 melanoma cell migration via the phosphatidylinositol 3-kinase/Akt/Rac1 signal pathway. Exp. Mol. Med. 40 (5), 486–494. https://doi.org/10.3858/emm.2008.40.5.486, 2008 40:5.

Silverstein, R.W., Bassler, G.C., 1962. Spectrometric identification of organic compounds. J. Chem. Educ. 39 (11), 546–553. https://doi.org/10.1021/ED039P546.

Simone, D.A., Baumann, T.K., LaMotte, R.H., 1989. Dose-dependent pain and mechanical hyperalgesia in humans after intradermal injection of capsaicin. Pain 38 (1), 99–107. https://doi.org/10.1016/0304-3959(89)90079-1.

Siudem, P., Paradowska, K., Bukowicki, J., 2017. Conformational analysis of capsaicin using 13C, 15N MAS NMR, GIAO DFT and GA calculations. J. Mol. Struct. 1146, 773–781. https://doi.org/10.1016/J.MOLSTRUC.2017.05.142.

Spackman, M.A., Byrom, P.G., 1997. A novel definition of a molecule in a crystal. Chem. Phys. Lett. 267 (3–4), 215–220. https://doi.org/10.1016/S0009-2614(97)00100-0.

Spackman, M.A., Jayatilaka, D., 2009. Hirshfeld surface analysis. CrystEngComm 11 (1), 19–32. https://doi.org/10.1039/B818330A.

Spackman, M.A., McKinnon, J.J., 2002. Fingerprinting intermolecular interactions in molecular crystals. CrystEngComm 4 (66), 378–392. https://doi.org/10.1039/B203191B.

Späth, E., Darling, S.F., 1930. Synthese des Capsaicins. Ber. Dtsch. Chem. Ges. 63 (3), 737–743. https://doi.org/10.1002/CBER.19300630331.

Tian, K., Wang, W., Yao, Y., Nie, X., Lu, A., Wu, Y., Han, C., 2018. Rapid identification of gutter oil by detecting the capsaicin using surface enhanced Raman spectroscopy. J. Raman Spectrosc. 49 (3), 472–481. https://doi.org/10.1002/JRS.5306.

Toth, B., Rogan, E., Walker, B., 1984. Tumorigenicity and mutagenicity studies with capsaicin of hot peppers. Anticancer Res. 4 (3), 117–119.

Turner, M., Kinnon, J.M., Wolff, S., Grimwood, D., Spackman, P., Jayatilaka, D., Spackman, M., 2017. CrystalExplorer17. University of Western Australia.

Vadivelu, N., Mitra, S., Narayan, D., 2010. Recent advances in postoperative pain management. Yale J. Biol. Med. 83 (1), 11.

Van Gisbergen, S.J.A., Osinga, V.P., Gritsenko, O.V., Van Leeuwen, R., Snijders, J.G., Baerends, E.J., 1998. Improved density functional theory results for frequency-dependent polarizabilities, by the use of an exchange-correlation potential with correct asymptotic behavior. J. Chem. Phys. 105 (8), 3142. https://doi.org/10.1063/1.472182.

Venier, N.A., Yamamoto, T., Sugar, L.M., Adomat, H., Fleshner, N.E., Klotz, L.H., Venkateswaran, V., 2015. Capsaicin reduces the metastatic burden in the transgenic adenocarcinoma of the mouse prostate model. Prostate 75 (12), 1300–1311. https://doi.org/10.1002/PROS.23013.

Wolinski, K., Hinton, J.F., Pulay, P., 2002. Efficient implementation of the gauge-independent atomic orbital method for NMR chemical shift calculations. J. Am. Chem. Soc. 112 (23), 8251–8260. https://doi.org/10.1021/JA00179A005.

Young, M.K., Hwang, J.T., Dong, W.K., Yun, K.L., Ock, J.P., 2007. Involvement of AMPK signaling cascade in capsaicin-induced apoptosis of HT-29 colon cancer cells. Ann. N. Y. Acad. Sci. 1095 (1), 496–503. https://doi.org/10.1196/ANNALS.1397.053.